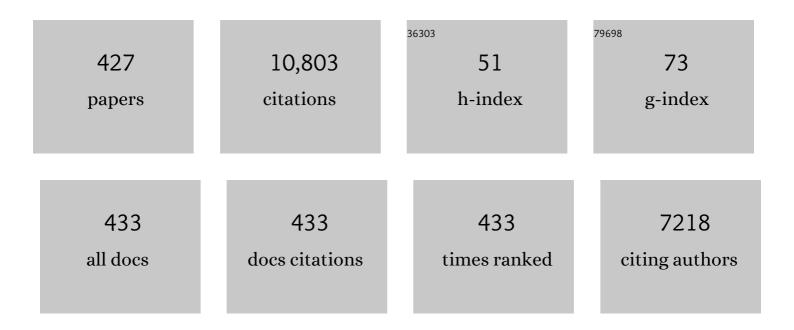
List of Publications by Year in descending order

Source: https://exaly.com/author-pdf/954075/publications.pdf Version: 2024-02-01



DEIVIANO LU

#	Article	IF	CITATIONS
1	Control of the Geometric Phase and Nonequivalence between Geometric-Phase Definitions in the Adiabatic Limit. Physical Review Letters, 2022, 128, 030401.	7.8	7
2	Interpreting attoclock experiments from the perspective of Bohmian trajectories. Physical Review A, 2022, 105, .	2.5	6
3	Double Rabi splitting in methylene blue dye-Ag nanocavity. Nanophotonics, 2022, 11, 603-611.	6.0	11
4	Fingerprint of the Interbond Electron Hopping in Second-Order Harmonic Generation. Physical Review Letters, 2022, 128, 027401.	7.8	6
5	Direct <i>In Situ</i> Measurement of an Ultrashort Pulse Using an Optical Hologram. Physical Review Applied, 2022, 17, .	3.8	2
6	Generation of 5.2 fs, energy scalable blue pulses. Optics Letters, 2022, 47, 389.	3.3	4
7	Rotational echo spectroscopy for accurate measurement of molecular alignment. Optics Letters, 2022, 47, 1033.	3.3	6
8	Multifunctional Chiral 2D Lead Halide Perovskites with Circularly Polarized Photoluminescence and Piezoelectric Energy Harvesting Properties. ACS Nano, 2022, 16, 3221-3230.	14.6	52
9	Spectral tuning of a broadband optical pulse via stimulated Raman scattering of a prealigned molecule. Physical Review A, 2022, 105, .	2.5	2
10	Zeeman effect in strong-field ionization. Physical Review A, 2022, 105, .	2.5	5
11	Resolving the time evolution of the dissociative nuclear wave packet in the repulsive state of <mml:math xmlns:mml="http://www.w3.org/1998/Math/MathML"><mml:msubsup><mml:mrow><mml:mi mathvariant="normal">H</mml:mi></mml:mrow><mml:mn>2</mml:mn><mml:mo>+</mml:mo></mml:msubsup><td>>ኛ/mml:n</td><td>1ath></td></mml:math>	>ኛ/mml:n	1ath>
12	Laser-induced deformation of atomic p _± orbitals in orthogonally polarized two-color laser fields. Journal of the Optical Society of America B: Optical Physics, 2022, 39, 1557.	2.1	1
13	Dangling Octahedra Enable Edge States in 2D Lead Halide Perovskites. Advanced Materials, 2022, 34, e2201666.	21.0	22
14	Two-photon-pumped amplified spontaneous emission from Ruddlesden-Popper perovskite flakes. Optics Express, 2022, 30, 21094.	3.4	4
15	Determination of transition dipole moments of solids with high-order harmonics driven by multicycle ultrashort pulses. Physical Review A, 2022, 105, .	2.5	12
16	Full experimental determination of tunneling time with attosecond-scale streaking method. Light: Science and Applications, 2022, 11, .	16.6	18
17	All-optical attosecond time domain interferometry. National Science Review, 2021, 8, nwaa211.	9.5	12
18	Large second-harmonic vortex beam generation with quasi-nonlinear spin–orbit interaction. Science Bulletin, 2021, 66, 449-456.	9.0	6

#	Article	lF	CITATIONS
19	Few-cycle optical pulse characterization under phase-mismatching. Optics Letters, 2021, 46, 548.	3.3	1
20	Method for high precision measurement of decaying dynamics using attosecond wave-mixing spectroscopy. Optics Express, 2021, 29, 2798.	3.4	4
21	Multilevel quantum interference in the formation of high-order fractional molecular alignment echoes. Optics Express, 2021, 29, 663.	3.4	6
22	Nonlinear detour phase holography. Nanoscale, 2021, 13, 2693-2702.	5.6	11
23	Curvature and Temperature Sensor Based on Anti-Resonant Effect Combined With Multimode Interference. IEEE Photonics Technology Letters, 2021, 33, 127-130.	2.5	12
24	Broadband frequency control of light using synthetic frequency lattices formed by four-wave-mixing Bragg scatterings. Physical Review A, 2021, 103, .	2.5	1
25	Real-time observation of frequency Bloch oscillations with fibre loop modulation. Light: Science and Applications, 2021, 10, 48.	16.6	30
26	Generation of elliptically polarized attosecond pulses in mixed gases. Physical Review A, 2021, 103, .	2.5	16
27	Temperature-independent ultra-sensitive refractive index sensor based on hollow-core silica tubes and tapers. Optics Express, 2021, 29, 10939.	3.4	13
28	Intensity and wavelength dependence of anisotropic nonlinear absorption inside MgO. Optical and Quantum Electronics, 2021, 53, 1.	3.3	3
29	Liao <i>etÂal.</i> Reply:. Physical Review Letters, 2021, 126, 109304.	7.8	0
30	Mapping time-dependent quasi-energies of laser dressed helium. Optics Express, 2021, 29, 11342.	3.4	5
31	Effects of quantum interferences among crystal-momentum-resolved electrons in solid high-order harmonic generation. Physical Review A, 2021, 103, .	2.5	6
32	Probing the launching position of the electron wave packet in molecule strong-field tunneling ionization. Science China: Physics, Mechanics and Astronomy, 2021, 64, 1.	5.1	11
33	Anomalous ellipticity dependence of the generation of near-threshold harmonics in noble gases. Physical Review A, 2021, 103, .	2.5	6
34	Intensity-dependent angular distribution of low-energy electrons generated by intense high-frequency laser pulse. Optics Express, 2021, 29, 16639.	3.4	10
35	Cutoff extension of high harmonics via resonant electron injection channels. Physical Review A, 2021, 103, .	2.5	7
36	Enhancement of the photocurrents injected in gapped graphene by the orthogonally polarized two-color laser field. Optics Express, 2021, 29, 17387.	3.4	3

#	Article	IF	CITATIONS
37	Dynamic Core Polarization in High Harmonic Generation from Solids: The Example of MgO Crystals. Physical Review Letters, 2021, 126, 187401.	7.8	12
38	Resolving and weighing the quantum orbits in strong-field tunneling ionization. Advanced Photonics, 2021, 3, .	11.8	17
39	Resonant Nonlinear Synthetic Metasurface with Combined Phase and Amplitude Modulations. Laser and Photonics Reviews, 2021, 15, 2100031.	8.7	10
40	Two-center interference and stereo Wigner time delay in photoionization of asymmetric molecules. Physical Review A, 2021, 104, .	2.5	8
41	Sensitivity-enhanced temperature sensor based on encapsulated S-taper fiber Modal interferometer. Optics and Laser Technology, 2021, 139, 106933.	4.6	24
42	Ultrafast imaging of spontaneous symmetry breaking in a photoionized molecular system. Nature Communications, 2021, 12, 4233.	12.8	12
43	Non-Hermitian flat bands in rhombic microring resonator arrays. Optics Express, 2021, 29, 24373.	3.4	14
44	Resolving the polarization of high-order harmonic generation by temporal multislit interferometry. Physical Review A, 2021, 104, .	2.5	2
45	Controllable Plexcitonic Coupling in a WS ₂ -Ag Nanocavity with Solvents. ACS Applied Materials & Interfaces, 2021, 13, 43554-43561.	8.0	5
46	Simplified highly-sensitive gas pressure sensor based on harmonic Vernier effect. Optics and Laser Technology, 2021, 140, 107007.	4.6	51
47	Tracing the electron motion in H2+ using attosecond photoelectron spectroscopy. Journal of Physics B: Atomic, Molecular and Optical Physics, 2021, 54, 165601.	1.5	0
48	Fiber tip Michelson interferometer for temperature sensing based on polymer-filled suspended core fiber. Optics and Laser Technology, 2021, 141, 107147.	4.6	21
49	Orientation dependence of high-order harmonic generation in graphene. Physical Review A, 2021, 104, .	2.5	11
50	Resonance-induced ionization enhancement and suppression of circular states of the hydrogen atom in strong laser fields. Physical Review A, 2021, 104, .	2.5	2
51	Extracting the phase distribution of the electron wave packet ionized by an elliptically polarized laser pulse. Frontiers of Physics, 2021, 16, 1.	5.0	4
52	Photoelectron holography in strong-field tunneling ionization by a spatially inhomogeneous field. Physical Review A, 2021, 104, .	2.5	8
53	Frequency manipulation of topological surface states by Weyl phase transitions. Optics Letters, 2021, 46, 5719.	3.3	3
54	Nondipole effects on the double-slit interference in molecular ionization by xuv pulses. Optics Express, 2021, 29, 38758.	3.4	5

#	Article	IF	CITATIONS
55	Analyzing the electron trajectories in strong-field tunneling ionization with the phase-of-the-phase spectroscopy. Optics Express, 2021, 29, 37927.	3.4	2
56	Attosecond photoemission delay in the inhomogeneous field. Optics Express, 2021, 29, 39729.	3.4	1
57	Huygens-Fresnel Picture for High Harmonic Generation in Solids. Physical Review Letters, 2021, 127, 223201.	7.8	18
58	Highly Tunable Enhancement and Switching of Nonlinear Emission from All-Inorganic Lead Halide Perovskites via Electric Field. Nano Letters, 2021, 21, 10230-10237.	9.1	12
59	Picometer-Resolved Photoemission Position within the Molecule by Strong-Field Photoelectron Holography. Physical Review Letters, 2021, 127, 263202.	7.8	12
60	In-situ adjustable fiber-optic piezometer based on parallelly structured external Fabry-Perot interferometers with Vernier effect and its harmonics. Optics Express, 2021, 29, 42800.	3.4	17
61	Gigahertz coherent longitudinal acoustic phonons in GaAs Single crystals with different orientations. Optics Communications, 2020, 461, 125257.	2.1	3
62	Temporal Imaging Using Dispersive Gradient-Index Time Lenses. Journal of Lightwave Technology, 2020, 38, 2383-2391.	4.6	3
63	Directional Excitation of Surface Plasmon Polaritons by Circularly Polarized Vortex Beams. Plasmonics, 2020, 15, 727-734.	3.4	2
64	Two-photon-pumped high-quality, single-mode vertical cavity lasing based on perovskite monocrystalline films. Nano Energy, 2020, 68, 104334.	16.0	29
65	Probing laser-driven bound-state dynamics using attosecond streaking spectroscopy. Physical Review A, 2020, 102, .	2.5	2
66	Perturbed ac Stark Effect for Attosecond Optical-Waveform Sampling. Physical Review Applied, 2020, 13, .	3.8	17
67	Photoelectron ionization time of aligned molecules clocked by attosecond angular streaking. Physical Review A, 2020, 102, .	2.5	14
68	Giant Quantum Yield Enhancement in CdS/MgF ₂ /Ag Hybrid Nanobelt under Two-Photon Excitation. ACS Photonics, 2020, 7, 2987-2994.	6.6	2
69	Elliptical isolated attosecond-pulse generation from an atom in a linear laser field. Physical Review A, 2020, 102, .	2.5	19
70	Ellipticity control of high-order harmonic generation with nearly orthogonal two-color laser fields. Physical Review A, 2020, 101, .	2.5	29
71	Near-circularly-polarized attosecond pulse generation from carbon monoxide molecules with a combination of linearly and circularly polarized fields. Physical Review A, 2020, 101, .	2.5	13
72	Chirality-selected second-harmonic holography with phase and binary amplitude manipulation. Nanoscale, 2020, 12, 13330-13337.	5.6	14

#	Article	IF	CITATIONS
73	Capillary Fiber Bragg Grating Fabricated by Femtosecond Laser for Sensing Applications. IEEE Photonics Technology Letters, 2020, 32, 783-786.	2.5	3
74	Scattering singularities of optical waveguides under complex modulation. Physical Review A, 2020, 101,	2.5	8
75	Retrieval of full angular- and energy-dependent complex transition dipoles in the molecular frame from laser-induced high-order harmonic signals with aligned molecules. Physical Review A, 2020, 101, .	2.5	12
76	Thermal Transport Engineering in Hybrid Organic–Inorganic Perovskite Phononic Crystals. Journal of Physical Chemistry Letters, 2020, 11, 5728-5733.	4.6	9
77	Improved photoemission and stability of 2D organic-inorganic lead iodide perovskite films by polymer passivation. Nanotechnology, 2020, 31, 42LT01.	2.6	14
78	Smart optically induced nonlinear photonic crystals for frequency conversion and control. Applied Physics Letters, 2020, 116, .	3.3	11
79	Interference effect in high-order harmonic generation from degenerate current-carrying orbitals of polyatomic molecules. Physical Review A, 2020, 101, .	2.5	11
80	Discrete diffraction and Bloch oscillations in non-Hermitian frequency lattices induced by complex photonic gauge fields. Physical Review B, 2020, 101, .	3.2	27
81	Resolving strong-field tunneling ionization with a temporal double-slit interferometer. Physical Review A, 2020, 101, .	2.5	10
82	Photoinduced Trap Passivation for Enhanced Photoluminescence in 2D Organic–Inorganic Hybrid Perovskites. Advanced Optical Materials, 2020, 8, 1901695.	7.3	14
83	Harmonic Resonance Enhanced Second-Harmonic Generation in the Monolayer WS ₂ –Ag Nanocavity. ACS Photonics, 2020, 7, 562-568.	6.6	53
84	Generation of Nearâ€Circularly Polarized Attosecond Pulse with Tunable Helicity by Unidirectionally Rotating Laser Field. Annalen Der Physik, 2020, 532, 1900570.	2.4	9
85	Efficient Mode Transfer on a Compact Silicon Chip by Encircling Moving Exceptional Points. Physical Review Letters, 2020, 124, 153903.	7.8	58
86	Determination of Electron Band Structure using Temporal Interferometry. Physical Review Letters, 2020, 124, 157403.	7.8	54
87	Towards atom-scale spin-selective electron emitters based on strong-field Freeman resonant ionization. Physical Review A, 2020, 102, .	2.5	8
88	Two-dimensional non-Hermitian Skin Effect in a Synthetic Photonic Lattice. Physical Review Applied, 2020, 14, .	3.8	66
89	Generation of second harmonic Bessel beams through hybrid meta-axicons. Optics Express, 2020, 28, 3179.	3.4	6
90	Revealing the effect of atomic orbitals on the phase distribution of an ionizing electron wave packet with circularly polarized two-color laser fields. Optics Express, 2020, 28, 12439.	3.4	6

#	Article	IF	CITATIONS
91	Generation of isolated circularly polarized attosecond pulses by three-color laser field mixing. Optics Express, 2020, 28, 15874.	3.4	19
92	Measuring the rotational temperature and pump intensity in molecular alignment experiments via high harmonic generation. Optics Express, 2020, 28, 21182.	3.4	16
93	All-optical frequency-resolved optical gating for isolated attosecond pulse reconstruction. Optics Letters, 2020, 45, 567.	3.3	25
94	Proposal for detecting ring current via electron vortices. Optics Letters, 2020, 45, 1383.	3.3	6
95	Structuring Nonlinear Wavefront Emitted from Monolayer Transition-Metal Dichalcogenides. Research, 2020, 2020, 9085782.	5.7	40
96	Non-dipole effect in vortex high-order harmonic generation. Journal of Physics B: Atomic, Molecular and Optical Physics, 2020, 53, 215601.	1.5	1
97	Efficient Spectrum Reshaping with Photonic Gauge Potentials in Resonantly Modulated Fiber-Loop Circuits. Physical Review Applied, 2019, 12, .	3.8	5
98	Nonlinear wavefront shaping with opticallyÂinduced three-dimensional nonlinear photonic crystals. Nature Communications, 2019, 10, 3208.	12.8	68
99	Influences of Ga Doping on Crystal Structure and Polarimetric Pattern of SHG in ZnO Nanofilms. Nanomaterials, 2019, 9, 905.	4.1	5
100	Nonadiabaticity-induced ionization time shift in strong-field tunneling ionization. Physical Review A, 2019, 100, .	2.5	10
101	Tuning Pressure-Induced Phase Transitions, Amorphization, and Excitonic Emissions of 2D Hybrid Perovskites via Varying Organic Amine Cations. Journal of Physical Chemistry C, 2019, 123, 22491-22498.	3.1	19
102	Asymmetry of the photoelectron momentum distribution from molecular ionization in elliptically polarized laser pulses. Physical Review A, 2019, 99, .	2.5	13
103	Negative area compressibility of a hydrogen-bonded two-dimensional material. Chemical Science, 2019, 10, 1309-1315.	7.4	24
104	Exit momentum and instantaneous ionization rate of nonadiabatic tunneling ionization in elliptically polarized laser fields. Physical Review A, 2019, 99, .	2.5	32
105	Spectrum Manipulation for Sound with Effective Gauge Fields in Cascading Temporally Modulated Waveguides. Physical Review Applied, 2019, 11, .	3.8	4
106	Direct imaging of molecular rotation with high-order-harmonic generation. Physical Review A, 2019, 99, .	2.5	39
107	Accelerating self-imaging effect for Airy pulse trains. Physical Review A, 2019, 99, .	2.5	9
108	Photoelectron Holographic Interferometry to Probe the Longitudinal Momentum Offset at the Tunnel Exit. Physical Review Letters, 2019, 122, 183202.	7.8	51

#	Article	IF	CITATIONS
109	Reciprocal-Space-Trajectory Perspective on High-Harmonic Generation in Solids. Physical Review Letters, 2019, 122, 193901.	7.8	96
110	Photoelectron holographic interferences from multiple returning in strong-field tunneling ionization. Optical and Quantum Electronics, 2019, 51, 1.	3.3	13
111	Elastic and hydrostatic behaviour of a zinc dietary supplement, zinc glycinate hydrate. RSC Advances, 2019, 9, 13153-13158.	3.6	6
112	Time-resolving tunneling ionization via strong-field photoelectron holography. Physical Review A, 2019, 99, .	2.5	30
113	Orientation dependence of high-order harmonic generation in nanowire. Physical Review A, 2019, 99, .	2.5	32
114	Gigahertz acoustic vibrations of Ga-doped ZnO nanoparticle array. Nanotechnology, 2019, 30, 305201.	2.6	18
115	Coherent steering of nonlinear chiral valley photons with a synthetic Au–WS2 metasurface. Nature Photonics, 2019, 13, 467-472.	31.4	236
116	Detecting and Characterizing the Nonadiabaticity of Laser-Induced Quantum Tunneling. Physical Review Letters, 2019, 122, 053202.	7.8	40
117	Semiclassical analysis of photoelectron interference in a synthesized two-color laser pulse. Physical Review A, 2019, 100, .	2.5	23
118	An inline fiber curvature sensor based on anti-resonant reflecting guidance in silica tube. Optics and Laser Technology, 2019, 111, 407-410.	4.6	28
119	Enhancement of the Second Harmonic Generation from WS ₂ Monolayers by Cooperating with Dielectric Microspheres. Advanced Optical Materials, 2019, 7, 1801270.	7.3	28
120	Timing the release of the correlated electrons in strong-field nonsequential double ionization by circularly polarized two-color laser fields. Optics Express, 2019, 27, 1825.	3.4	36
121	Internal collision induced strong-field nonsequential double ionization in molecules. Optics Express, 2019, 27, 6415.	3.4	20
122	ldentification of tunneling and multiphoton ionization in intermediate Keldysh parameter regime. Optics Express, 2019, 27, 6471.	3.4	29
123	Topological bound modes in anti-PT-symmetric optical waveguide arrays. Optics Express, 2019, 27, 13858.	3.4	64
124	Frustrated tunneling ionization in the elliptically polarized strong laser fields. Optics Express, 2019, 27, 21689.	3.4	36
125	All-optical measurement of high-order fractional molecular echoes by high-order harmonic generation. Optics Express, 2019, 27, 30172.	3.4	33
126	Enhanced optoelectronic performance of 2D organic-inorganic hybrid perovskite through light-illumination. Optics Express, 2019, 27, 30618.	3.4	6

PEIXIANG LU

#	Article	IF	CITATIONS
127	Two-dimensional photoelectron holography in strong-field tunneling ionization by counter rotating two-color circularly polarized laser pulses. Optics Express, 2019, 27, 32193.	3.4	23
128	Channel-closing effects of electronic excitation in solids. Optics Express, 2019, 27, 37224.	3.4	7
129	Low-energy photoelectron interference structure in attosecond streaking. Optics Express, 2019, 27, 37736.	3.4	9
130	Coulomb focusing in retrapped ionization with near-circularly polarized laser field. Optics Express, 2019, 27, 38116.	3.4	12
131	Discrete refraction and reflection in temporal lattice heterostructures. Optics Letters, 2019, 44, 363.	3.3	13
132	Bloch oscillations in photonic spectral lattices through phase-mismatched four-wave mixing. Optics Letters, 2019, 44, 5430.	3.3	14
133	Few-cycle 19-μm pulse generation via collinear spectrum synthesis in multiple-crystal OPA. Optics Letters, 2019, 44, 3438.	3.3	6
134	Topological interface modes in graphene multilayer arrays. Optics and Laser Technology, 2018, 103, 272-278.	4.6	31
135	Strong-field photoelectron holography of atoms by bicircular two-color laser pulses. Physical Review A, 2018, 97, .	2.5	39
136	Identifying the contributions of multiple-returning recollision orbits in strong-field above-threshold ionization. Optical and Quantum Electronics, 2018, 50, 1.	3.3	30
137	Resonance-modulated wavelength scaling of high-order-harmonic generation from <mml:math xmlns:mml="http://www.w3.org/1998/Math/MathML"><mml:mrow><mml:msub><mml:mi mathvariant="normal">H<mml:mn>2</mml:mn></mml:mi </mml:msub><mml:msup><mml:mrow /><mml:mo>+</mml:mo></mml:mrow </mml:msup></mml:mrow>. Physical Review A, 2018, 97, .</mml:math 	2.5	12
138	Cooperative Enhancement of Twoâ€Photonâ€Absorptionâ€Induced Photoluminescence from a 2D Perovskiteâ€Microsphere Hybrid Dielectric Structure. Advanced Functional Materials, 2018, 28, 1707550.	14.9	70
139	Tungsten Disulfide–Gold Nanohole Hybrid Metasurfaces for Nonlinear Metalenses in the Visible Region. Nano Letters, 2018, 18, 1344-1350.	9.1	83
140	Rabi oscillation in few-photon double ionization through doubly excited states. Physical Review A, 2018, 97, .	2.5	30
141	Jahn–Teller Effect on Framework Flexibility of Hybrid Organic–Inorganic Perovskites. Journal of Physical Chemistry Letters, 2018, 9, 751-755.	4.6	47
142	Optical Imaginary Directional Couplers. Journal of Lightwave Technology, 2018, 36, 2510-2516.	4.6	35
143	Spectrum Control through Discrete Frequency Diffraction in the Presence of Photonic Gauge Potentials. Physical Review Letters, 2018, 120, 133901.	7.8	92
144	Direct Visualization of Valence Electron Motion Using Strong-Field Photoelectron Holography. Physical Review Letters, 2018, 120, 133204.	7.8	90

#	Article	IF	CITATIONS
145	Monitoring ultrafast vibrational dynamics of isotopic molecules with frequency modulation of high-order harmonics. Nature Communications, 2018, 9, 1108.	12.8	102
146	Tunable few-cycle pulses from a dual-chirped optical parametric amplifier pumped by broadband laser. Optics and Laser Technology, 2018, 98, 169-177.	4.6	30
147	Elastic properties and thermal expansion of lead-free halide double perovskite Cs2AgBiBr6. Computational Materials Science, 2018, 141, 49-58.	3.0	87
148	Momentum gate for tunneling electrons with a circularly polarized control field. Physical Review A, 2018, 98, .	2.5	7
149	Quantifying the Exfoliation Ease Level of 2D Materials via Mechanical Anisotropy. Chemistry of Materials, 2018, 30, 8732-8738.	6.7	49
150	Imaging charge migration in the asymmetric molecule with the holographic interference in strong-field tunneling ionization. Journal of Physics B: Atomic, Molecular and Optical Physics, 2018, 51, 245602.	1.5	3
151	Wavelength dependence of high-order harmonic yields in solids. Physical Review A, 2018, 98, .	2.5	10
152	Determination of the Ionization Time Using Attosecond Photoelectron Interferometry. Physical Review Letters, 2018, 121, 253203.	7.8	69
153	<mml:math xmlns:mml="http://www.w3.org/1998/Math/MathML"> <mml:mrow> <mml:mi mathvariant="script">P <mml:mi mathvariant="script">T</mml:mi> </mml:mi </mml:mrow> </mml:math> -symmetric Talbot effect in a temporal mesh lattice. Physical Review A, 2018, 98, .	2.5	15
154	Real-Time Observation of Molecular Spinning with Angular High-Harmonic Spectroscopy. Physical Review Letters, 2018, 121, 163201.	7.8	60
155	Rabi Splitting in a Plasmonic Nanocavity Coupled to a WS ₂ Monolayer at Room Temperature. ACS Photonics, 2018, 5, 3970-3976.	6.6	120
156	An Unusual Phase Transition Driven by Vibrational Entropy Changes in a Hybrid Organic–Inorganic Perovskite. Angewandte Chemie, 2018, 130, 9070-9074.	2.0	10
157	An Unusual Phase Transition Driven by Vibrational Entropy Changes in a Hybrid Organic–Inorganic Perovskite. Angewandte Chemie - International Edition, 2018, 57, 8932-8936.	13.8	46
158	Scaling Law of High Harmonic Generation in the Framework of Photon Channels. Physical Review Letters, 2018, 120, 223203.	7.8	27
159	Photoelectron holography and forward scattering in atomic ionization by elliptically polarized laser pulses. Optics Letters, 2018, 43, 3220.	3.3	20
160	Single-shot molecular orbital tomography with orthogonal two-color fields. Optics Express, 2018, 26, 2775.	3.4	31
161	Giant Goos-Hächen shifts in non-Hermitian dielectric multilayers incorporated with graphene. Optics Express, 2018, 26, 2817.	3.4	34
162	Collisional dynamics in laser-induced plasmas: evidence for electron-impact excitation. Optics Express, 2018, 26, 10392.	3.4	1

#	Article	IF	CITATIONS
163	Controlling nonsequential double ionization of Ne with parallel-polarized two-color laser pulses. Optics Express, 2018, 26, 13666.	3.4	14
164	High-efficiency energy transfer in perovskite heterostructures. Optics Express, 2018, 26, 18448.	3.4	23
165	Tomography of asymmetric molecular orbitals with a one-color inhomogeneous field. Optics Letters, 2018, 43, 931.	3.3	25
166	Ultrabroadband microjoule 18  μm laser pulse from a single-stage broadband pumped OPA. Optics Let 2018, 43, 3706.	ters. 3.3	9
167	Nearâ€Field Characterization of Graphene Plasmons by Photoâ€Induced Force Microscopy. Laser and Photonics Reviews, 2018, 12, 1800040.	8.7	26
168	Ultrafast Mid-IR Laser Pulses Generation via Chirp Manipulated Optical Parametric Amplification. Applied Sciences (Switzerland), 2018, 8, 744.	2.5	8
169	Attosecond control of correlated electron dynamics in strong-field nonsequential double ionization by parallel two-color pulses. Optics and Laser Technology, 2018, 108, 235-240.	4.6	23
170	Photonic Weyl phase transition in dynamically modulated brick-wall waveguide arrays. Optics Express, 2018, 26, 20929.	3.4	14
171	Probing electron–atom collision dynamics in gas plasma by high-order harmonic spectroscopy. Optics Letters, 2018, 43, 1970.	3.3	7
172	Subpetahertz helicity-modulated high-order harmonic radiation. Physical Review A, 2018, 98, .	2.5	11
173	Airy pulse shaping using time-dependent power-law potentials. Physical Review A, 2018, 97, .	2.5	20
174	Effective electric-field force for a photon in a synthetic frequency lattice created in a waveguide modulator. Physical Review A, 2018, 97, .	2.5	34
175	Discrete temporal Talbot effect in synthetic mesh lattices. Optics Express, 2018, 26, 19235.	3.4	21
176	Accurate measurement of laser intensity using photoelectron interference in strong-field tunneling ionization. Optics Express, 2018, 26, 20063.	3.4	11
177	Method for direct observation of Bloch oscillations in semiconductors. Optics Express, 2018, 26, 23844.	3.4	13
178	Frequency diffraction management through arbitrary engineering of photonic band structures. Optics Express, 2018, 26, 25721.	3.4	10
179	Steering electron correlation time by elliptically polarized femtosecond laser pulses. Optics Express, 2018, 26, 33400.	3.4	3
180	Carrier-envelope phase-dependent molecular high-order harmonic generation from H2+ in a multi-cycle regime. Optics Express, 2018, 26, 33440.	3.4	2

#	Article	IF	CITATIONS
181	Rabi Oscillations of Plasmonic Supermodes in Graphene Multilayer Arrays. IEEE Journal of Selected Topics in Quantum Electronics, 2017, 23, 125-129.	2.9	27
182	Plasmon assisted enhanced second-harmonic generation in single hybrid Au/ZnS nanowires. Optical Materials, 2017, 64, 257-261.	3.6	18
183	Giant Twoâ€Photon Absorption and Its Saturation in 2D Organic–Inorganic Perovskite. Advanced Optical Materials, 2017, 5, 1601045.	7.3	175
184	Controllable alignment of elongated microorganisms in 3D microspace using electrofluidic devices manufactured by hybrid femtosecond laser microfabrication. Microsystems and Nanoengineering, 2017, 3, 16078.	7.0	28
185	Correlated electron-nuclear dynamics in above-threshold multiphoton ionization of asymmetric molecule. Scientific Reports, 2017, 7, 42585.	3.3	17
186	Surface Plasmonic Lattice Solitons in Semi-Infinite Graphene Sheet Arrays. Journal of Lightwave Technology, 2017, 35, 2960-2965.	4.6	37
187	Revealing the target structure information encoded in strong-field photoelectron hologram. Optical and Quantum Electronics, 2017, 49, 1.	3.3	23
188	Probing the <mml:math xmlns:mml="http://www.w3.org/1998/Math/MathML"><mml:mrow><mml:mi>Ï€</mml:mi><mml:mo>â^'transitions in conjugated compounds with an infrared femtosecond laser. Physical Review A, 2017, 95, .</mml:mo></mml:mrow></mml:math 	mo 2.5 mml	:msup> <mml< td=""></mml<>
189	Nonsequential double ionization of Xe by mid-infrared laser pulses. Optical and Quantum Electronics, 2017, 49, 1.	3.3	25
190	Numerical Study on Plasmonic Absorption Enhancement by a Rippled Graphene Sheet. Journal of Lightwave Technology, 2017, 35, 320-324.	4.6	47
191	Concentrated secondâ€harmonic generation from a single Alâ€covered ZnS nanobelt. Laser and Photonics Reviews, 2017, 11, 1600263.	8.7	6
192	Universal time delay in the recollision impact ionization pathway of strong-field nonsequential double ionization. Journal of Physics B: Atomic, Molecular and Optical Physics, 2017, 50, 225601.	1.5	7
193	Angular-dependent asymmetries of above-threshold ionization in a two-color laser field. Physical Review A, 2017, 96, .	2.5	18
194	Macroscopic effect of plasmon-driven high-order-harmonic generation. Physical Review A, 2017, 96, .	2.5	15
195	Attosecond Probing of Nuclear Dynamics with Trajectory-Resolved High-Harmonic Spectroscopy. Physical Review Letters, 2017, 119, 033201.	7.8	111
196	Asymmetric molecular-orbital tomography by manipulating electron trajectories. Physical Review A, 2017, 96, .	2.5	6
197	High-order-harmonic generation of a doped semiconductor. Physical Review A, 2017, 96, .	2.5	54
198	Correlated electron dynamics in strong-field nonsequential double ionization of Mg. Journal of Chemical Physics, 2017, 147, 174302.	3.0	6

#	Article	IF	CITATIONS
199	Time-dependent population imaging for high-order-harmonic generation in solids. Physical Review A, 2017, 95, .	2.5	71
200	Diffractive molecular-orbital tomography. Physical Review A, 2017, 95, .	2.5	32
201	Topological mode switching in a graphene doublet with exceptional points. Optical and Quantum Electronics, 2017, 49, 1.	3.3	28
202	Anti-Resonant Reflecting Guidance in Silica Tube for High Temperature Sensing. IEEE Photonics Technology Letters, 2017, 29, 2135-2138.	2.5	23
203	Plasmon-shaped polarization gating for high-order-harmonic generation. Physical Review A, 2017, 96, .	2.5	2
204	Energy-dependent angular shifts in the photoelectron momentum distribution for atoms in elliptically polarized laser pulses. Physical Review A, 2017, 96, .	2.5	27
205	Diffractive imaging of molecular orbital. , 2017, , .		0
206	Asymmetric plasmonic supermodes in nonlinear graphene multilayers. Optics Express, 2017, 25, 1234.	3.4	10
207	Exceptional points in Fano-resonant graphene metamaterials. Optics Express, 2017, 25, 7203.	3.4	41
208	Topological edge modes in non-Hermitian plasmonic waveguide arrays. Optics Express, 2017, 25, 11132.	3.4	40
209	Carrier-envelope phase dependent photoelectron energy spectra in low intensity regime. Optics Express, 2017, 25, 11233.	3.4	16
210	Surface vector plasmonic lattice solitons in semi-infinite graphene-pair arrays. Optics Express, 2017, 25, 20708.	3.4	4
211	High harmonic generation from axial chiral molecules. Optics Express, 2017, 25, 23502.	3.4	14
212	Wavelength scaling of the cutoff energy in the solid high harmonic generation. Optics Express, 2017, 25, 29216.	3.4	26
213	Quantitatively extracting the contribution of asymmetric local-field to χ^(2) in cross-shaped Ag nanoholes. Optics Express, 2017, 25, 1296.	3.4	4
214	Dissection of electron correlation in strong-field sequential double ionization using a classical model. Optics Express, 2017, 25, 8450.	3.4	21
215	Dual-wavelength Highly-sensitive refractive index sensor. Optics Express, 2017, 25, 14389.	3.4	36
216	Resonance enhanced high-order harmonic generation in H2+ by two sequential laser pulses. Optics Express, 2017, 25, 17777.	3.4	26

PEIXIANG LU

#	Article	IF	CITATIONS
217	Ellipticity-tunable attosecond XUV pulse generation with a rotating bichromatic circularly polarized laser field. Optics Letters, 2017, 42, 1027.	3.3	56
218	Ultrabroadband tunable OPA design using a spectrally broadened pump source. Optics Letters, 2017, 42, 3367.	3.3	24
219	Enhanced plasmonic nanofocusing of terahertz waves in tapered graphene multilayers. Optics Express, 2016, 24, 14765.	3.4	18
220	Identifying backward-rescattering photoelectron hologram with orthogonal two-color laser fields. Optics Express, 2016, 24, 23697.	3.4	20
221	Anomalous circular dichroism in high harmonic generation of stereoisomers with two chiral centers. Optics Express, 2016, 24, 24824.	3.4	9
222	Intra-half-cycle interference of low-energy photoelectron in strong midinfrared laser fields. Optics Express, 2016, 24, 27726.	3.4	21
223	Antiresonant reflecting guidance mechanism in hollow-core fiber for gas pressure sensing. Optics Express, 2016, 24, 27890.	3.4	98
224	Highly Sensitive Detection of the Lattice Distortion in Single Bent ZnO Nanowires by Second-Harmonic Generation Microscopy. ACS Photonics, 2016, 3, 1308-1314.	6.6	26
225	Non-reciprocal Phase Shift and Mode Modulation in Dynamic Graphene Waveguides. Journal of Lightwave Technology, 2016, , 1-1.	4.6	15
226	The contribution of the delayed ionization in strong-field nonsequential double ionization. Journal of Chemical Physics, 2016, 144, 024304.	3.0	22
227	Temperature Insensitive Liquid Level Sensor Based on Antiresonant Reflecting Guidance in Silica Tube. Journal of Lightwave Technology, 2016, 34, 5239-5243.	4.6	73
228	Time-resolved internal-electron-scattering effect ofH2+in enhanced ionization regions. Physical Review A, 2016, 94, .	2.5	12
229	Vector plasmonic lattice solitons in nonlinear graphene-pair arrays. Optics Letters, 2016, 41, 3619.	3.3	22
230	Tunable broadband intense IR pulse generation at non-degenerate wavelengths using group delay compensation in a dual-crystal OPA scheme. Optics Express, 2016, 24, 11187.	3.4	11
231	Unlocking the electrochemistry abilities of nanoscaled Na 2/3 Ni 1/4 Mn 3/4 O 2 thin films. Electrochimica Acta, 2016, 215, 550-555.	5.2	7
232	Extending plasma channel of filamentation with a multi-focal-length beam. Optics Express, 2016, 24, 4029.	3.4	21
233	Helicity sensitive enhancement of strong-field ionization in circularly polarized laser fields. Optics Express, 2016, 24, 4196.	3.4	38
234	Exceptional Points and Asymmetric Mode Switching in Plasmonic Waveguides. Journal of Lightwave Technology, 2016, 34, 5258-5262.	4.6	71

PEIXIANG LU

#	Article	IF	CITATIONS
235	Selection rules of high-order-harmonic generation: Symmetries of molecules and laser fields. Physical Review A, 2016, 94, .	2.5	80
236	Plasmonic Zener tunneling in binary graphene sheet arrays. Optics Letters, 2016, 41, 2978.	3.3	7
237	Counterintuitive energy shifts in joint electron–nuclear-energy spectra of strong-field fragmentation ofH2+. Physical Review A, 2016, 93, .	2.5	19
238	Multiple recollisions in strong-field nonsequential double ionization. Physical Review A, 2016, 93, .	2.5	52
239	Temporal and spatial manipulation of the recolliding wave packet in strong-field photoelectron holography. Physical Review A, 2016, 93, .	2.5	39
240	Helicity reversion in high-order-harmonic generation driven by bichromatic counter-rotating circularly polarized laser fields. Physical Review A, 2016, 94, .	2.5	19
241	Coulomb-corrected molecular orbital tomography of nitrogen. Scientific Reports, 2016, 6, 23236.	3.3	30
242	Multi-Components Interferometer Based on Partially Filled Dual-Core Photonic Crystal Fiber for Temperature and Strain Sensing. IEEE Sensors Journal, 2016, 16, 6192-6196.	4.7	46
243	An aplanatic-lens velocity map imaging spectrometer with improved kinetic energy resolution for photoions. International Journal of Mass Spectrometry, 2016, 406, 55-61.	1.5	1
244	High pressure behaviour and elastic properties of a dense inorganic–organic framework. Dalton Transactions, 2016, 45, 4303-4308.	3.3	26
245	Surface plasmonic resonances and enhanced IR spectra in GZO nano-triangle arrays. Materials Letters, 2016, 172, 36-39.	2.6	9
246	Nonadiabatic tunnel ionization in strong circularly polarized laser fields: counterintuitive angular shifts in the photoelectron momentum distribution. Optics Express, 2015, 23, 28801.	3.4	25
247	Selective enhancement of resonant multiphoton ionization with strong laser fields. Physical Review A, 2015, 92, .	2.5	56
248	Isotropic Negative Area Compressibility over Large Pressure Range in Potassium Beryllium Fluoroborate and its Potential Applications in Deep Ultraviolet Region. Advanced Materials, 2015, 27, 4851-4857.	21.0	52
249	Plasmonic lattice solitons in nonlinear graphene sheet arrays. Optics Express, 2015, 23, 32679.	3.4	10
250	Maker fringes of different quantum paths in high-order harmonic generation. , 2015, , .		0
251	Plasmonic absorption enhancement in periodic cross-shaped graphene arrays. , 2015, , .		5
252	Rabi oscillations of surface plasmon polaritons in graphene-pair arrays. Optics Express, 2015, 23, 31136.	3.4	11

#	Article	IF	CITATIONS
253	Time-dependent phase matching of high-order-harmonic generation. Physical Review A, 2015, 92, .	2.5	27
254	Quantum path interference in the wavelength-dependent below-threshold harmonic generation. Physical Review A, 2015, 91, .	2.5	15
255	Molecular high-order-harmonic generation due to the recollision mechanism by a circularly polarized laser pulse. Physical Review A, 2015, 91, .	2.5	34
256	Ultrafast molecular orbital imaging based on attosecond photoelectron diffraction. Optics Express, 2015, 23, 10687.	3.4	15
257	Steering the electron in dissociating <mml:math xmlns:mml="http://www.w3.org/1998/Math/MathML"><mml:msup><mml:mrow><mml:msub><mml:mi mathvariant="normal">H<mml:mn>2</mml:mn></mml:mi </mml:msub></mml:mrow><mml:mo>+</mml:mo>manipulating two-state population dynamics by a weak low-frequency field. Physical Review A, 2015, 91,</mml:msup></mml:math 	n 2na :msup	> 14 mml:mat
258	Enhanced dissociation of H ₂ ⁺ into highly excited states by UV pulses. Molecular Physics, 2015, 113, 3247-3252.	1.7	6
259	Precise Determination of the Crystallographic Orientations in Single ZnS Nanowires by Second-Harmonic Generation Microscopy. Nano Letters, 2015, 15, 3351-3357.	9.1	66
260	Optimization of metal-enhanced fluorescence by different concentrations of gold-silica core–shell nanoparticles. Optics Communications, 2015, 349, 180-184.	2.1	9
261	Plasmonic Zitterbewegung in binary graphene sheet arrays. Optics Letters, 2015, 40, 2945.	3.3	7
262	Plasmonic absorption enhancement in periodic cross-shaped graphene arrays. Optics Express, 2015, 23, 8888.	3.4	185
263	Resolving subcycle electron emission in strong-field sequential double ionization. Optics Express, 2015, 23, 15774.	3.4	45
264	Angular distribution of ions and extreme ultraviolet emission in laser-produced tin droplet plasma. Journal of Applied Physics, 2015, 117, .	2.5	12
265	Two-photon-excited fluorescence resonance energy transfer in an aqueous system of CdTe quantum dots and Rhodamine B. Journal of Applied Physics, 2014, 116, .	2.5	13
266	Method to compensate the dispersion of kinetic energy resolution in a velocity map imaging spectrometer. Measurement Science and Technology, 2014, 25, 105202.	2.6	3
267	Plasmonic Bloch oscillations in monolayer graphene sheet arrays. Optics Letters, 2014, 39, 6827.	3.3	14
268	Sensitivity-Enhanced Pressure Sensor With Hollow-Core Photonic Crystal Fiber. Journal of Lightwave Technology, 2014, 32, 4637-4641.	4.6	19
269	Plasmon-negative refraction at the heterointerface of graphene sheet arrays. Optics Letters, 2014, 39, 5957.	3.3	22
270	Plasmonic routing in aperiodic graphene sheet arrays. Optics Letters, 2014, 39, 4867.	3.3	14

#	Article	IF	CITATIONS
271	Talbot effect in weakly coupled monolayer graphene sheet arrays. Optics Letters, 2014, 39, 3371.	3.3	28
272	High-order harmonic generation from Rydberg atoms in inhomogeneous fields. Optics Express, 2014, 22, 25909.	3.4	18
273	Generation of few-cycle infrared pulses from a degenerate dual-pump OPCPA. Optics Express, 2014, 22, 5544.	3.4	19
274	Probing rotational wave-packet dynamics with the structural minimum in high-order harmonic spectra. Optics Express, 2014, 22, 6362.	3.4	9
275	Molecular photoelectron holography by an attosecond XUV pulse in a strong infrared laser field. Optics Express, 2014, 22, 20421.	3.4	8
276	Low-loss plasmonic supermodes in graphene multilayers. Optics Express, 2014, 22, 25324.	3.4	39
277	Revealing the role of electron correlation in sequential double ionization. Physical Review A, 2014, 89, .	2.5	6
278	Tunable plasmon modes in single silver nanowire optical antennas characterized by far-field microscope polarization spectroscopy. Nanoscale, 2014, 6, 9192-9197.	5.6	18
279	Shaped multi-cycle two-color laser field for generating an intense isolated XUV pulse toward 100 attoseconds. Optics Express, 2014, 22, 13213.	3.4	28
280	Photoinduced energy transfer in a CdTe quantum dot–copper phthalocyanine system via two-photon excitation. Materials Letters, 2014, 132, 263-266.	2.6	12
281	Quantum trajectories for high-order-harmonic generation from multiple rescattering events in the long-wavelength regime. Physical Review A, 2014, 89, .	2.5	13
282	Subcycle Control of Electron-Electron Correlation in Double Ionization. Physical Review Letters, 2014, 112, 193002.	7.8	97
283	High-stability 5V spinel LiNi0.5Mn1.5O4 sputtered thin film electrodes by modifying with aluminium oxide. Electrochimica Acta, 2014, 136, 450-456.	5.2	31
284	Attosecond-resolved electron emission in nonsequential double ionization. Physical Review A, 2013, 88, .	2.5	9
285	Control of electron dynamics with a multicycle two-color spatially inhomogeneous field for efficient single-attosecond-pulse generation. Physical Review A, 2013, 88, .	2.5	30
286	Three-photon absorption of copper phthalocyanine solution by femtosecond Z-scan technique. Materials Letters, 2013, 111, 81-84.	2.6	13
287	High power and capacity of LiNi0.5Mn1.5O4 thin films cathodes prepared by pulsed laser deposition. Electrochimica Acta, 2013, 102, 416-422.	5.2	37
288	Tunable phase-matched attosecond-pulse generation with two-color Bessel-Gauss beams. Physical Review A, 2013, 87, .	2.5	7

#	Article	IF	CITATIONS
289	Tomographic reconstruction of molecular orbitals with twofold mirror antisymmetry: Overcoming the nodal plane problem. Physical Review A, 2013, 87, .	2.5	16
290	Optical limiting properties in copper oxide thin films under a high-repetition-rate femtosecond laser. Materials Letters, 2013, 91, 319-322.	2.6	35
291	Laterally Emitted Surface Second Harmonic Generation in a Single ZnTe Nanowire. Nano Letters, 2013, 13, 4224-4229.	9.1	50
292	Influence of large permanent dipoles on molecular orbital tomography. Optics Express, 2013, 21, 5255.	3.4	17
293	Ultra-broadband water window supercontinuum generation with high efficiency in a three-color laser field. Optics Express, 2013, 21, 2683.	3.4	18
294	Quantum-orbit analysis for yield and ellipticity of high order harmonic generation with elliptically polarized laser field. Optics Express, 2013, 21, 4896.	3.4	12
295	Anomalous isotopic effect on electron-directed reactivity by a 3-μm midinfrared pulse. Optics Express, 2013, 21, 5107.	3.4	13
296	Compact dual-crystal optical parametric amplification for broadband IR pulse generation using a collinear geometry. Optics Express, 2013, 21, 9491.	3.4	14
297	Contribution of recollision ionization to the cross-shaped structure in nonsequential double ionization. Optics Express, 2013, 21, 11382.	3.4	104
298	Anti-resonant reflecting guidance in alcohol-filled hollow core photonic crystal fiber for sensing applications. Optics Express, 2013, 21, 31690.	3.4	82
299	Correlated multielectron dynamics in mid-infrared laser pulse interactions with neon atoms. Optics Express, 2013, 21, 21433.	3.4	12
300	Direction-independent fiber inclinometer based on simplified hollow core photonic crystal fiber. Optics Letters, 2013, 38, 449.	3.3	39
301	Two-photon pumped lasing in a single CdS microwire. Applied Physics Letters, 2013, 102, .	3.3	21
302	Ultra-short isolated attosecond emission in mid-infrared inhomogeneous fields without CEP stabilization. Journal of Physics B: Atomic, Molecular and Optical Physics, 2013, 46, 145602.	1.5	79
303	Debris mitigation power of various buffer gases for CO ₂ laser produced tin plasmas. Journal Physics D: Applied Physics, 2012, 45, 475203.	2.8	7
304	Classical simulations of electron emissions from H2+ by circularly polarized laser pulses. Optics Express, 2012, 20, 11700.	3.4	19
305	Role of the Coulomb potential on the ellipticity in atomic high-order harmonics generation. Optics Express, 2012, 20, 16275.	3.4	16
306	Correlated electron dynamics in nonsequential double ionization of molecules by mid-infrared fields. Optics Express, 2012, 20, 19580.	3.4	10

#	Article	IF	CITATIONS
307	Imprints of the molecular-orbital geometry on the high-harmonic ellipticity. Optics Express, 2012, 20, 20181.	3.4	8
308	Broadband isolated attosecond pulse with high spatiotemporal quality in pre-excited medium by multi-cycle two-color fields. Optics Express, 2012, 20, 21346.	3.4	6
309	Enhanced anisotropy of the nonlinear absorption in the individual Au nanoparticles functionalized KNbO_3 sub-microwire. Optics Express, 2012, 20, 24209.	3.4	3
310	Tomographic imaging of asymmetric molecular orbitals with a two-color multicycle laser field. Optics Letters, 2012, 37, 5208.	3.3	28
311	Dramatic cutoff extension and broadband supercontinuum generation in multi-cycle two color pulses. Optics Express, 2012, 20, 9801.	3.4	11
312	Efficient generation of high beam-quality attosecond pulse with polarization-gating Bessel-Gauss beam from highly-ionized media. Optics Express, 2012, 20, 15427.	3.4	8
313	Revealing the multi-electron effects in sequential double ionization using classical simulations. Optics Express, 2012, 20, 20201.	3.4	27
314	Simple In-Line M–Z Interferometer Based on Dual-Core Photonic Crystal Fiber. IEEE Photonics Technology Letters, 2012, 24, 1768-1770.	2.5	10
315	Efficient generation of isolated attosecond pulses with high beam quality by two-color Bessel–Gauss beams. Optics Letters, 2012, 37, 238.	3.3	6
316	Enhancing electron localization in molecular dissociation by two-color mid- and near-infrared laser fields. Physical Review A, 2012, 86, .	2.5	42
317	Highly Birefringent Elliptical-Hole Microstructure Fibers With Low Confinement Loss. Journal of Lightwave Technology, 2012, 30, 3381-3386.	4.6	15
318	Classical description of strong-field double ionization by elliptical laser pulses. Physical Review A, 2012, 86, .	2.5	31
319	Resonantly enhanced optical nonlinearity in hybrid semiconductor quantum dot – metal nanoparticle structures. Applied Physics Letters, 2012, 100, .	3.3	39
320	Anisotropic Third-Order Optical Nonlinearity of a single ZnO Micro/Nanowire. Nano Letters, 2012, 12, 833-838.	9.1	60
321	Self-Cleaning Flexible Infrared Nanosensor Based on Carbon Nanoparticles. ACS Nano, 2011, 5, 4007-4013.	14.6	82
322	Prestressed Fiber Bragg Grating With High Temperature Stability. Journal of Lightwave Technology, 2011, 29, 1555-1559.	4.6	25
323	Two-center interference in high-order harmonic generation from heteronuclear diatomic molecules. Optics Express, 2011, 19, 436.	3.4	37
324	Bandwidth-narrowed Bragg gratings inscribed in double-cladding fiber by femtosecond laser. Optics Express, 2011, 19, 1734.	3.4	9

#	Article	IF	CITATIONS
325	Correlated electron dynamics in nonsequential double ionization by orthogonal two-color laser pulses. Optics Express, 2011, 19, 2301.	3.4	100
326	Improving the signal-to-noise ratio for circular polarizers consisting of helical metamaterials. Optics Express, 2011, 19, 4255.	3.4	54
327	Intense isolated attosecond pulse generation in pre-excited medium. Optics Express, 2011, 19, 4728.	3.4	11
328	The effect of molecular alignment on correlated electron dynamics in nonsequential double ionization. Optics Express, 2011, 19, 5627.	3.4	35
329	Dual-chirped optical parametric amplification for generating few hundred mJ infrared pulses. Optics Express, 2011, 19, 7190.	3.4	72
330	Spatial coherence control of xuv supercontinuum generation by two-color laser field. Optics Express, 2011, 19, 9986.	3.4	3
331	Molecular orbital imaging via above-threshold ionization with circularly polarized pulses. Optics Express, 2011, 19, 13722.	3.4	28
332	Bending insensitive sensors for strain and temperature measurements with Bragg gratings in Bragg fibers. Optics Express, 2011, 19, 13880.	3.4	45
333	Phase dependence of electron localization in HeH^2+ dissociation with an intense few-cycle laser pulse. Optics Express, 2011, 19, 20279.	3.4	23
334	Laser-polarization-dependent photoelectron angular distributions from polar molecules. Optics Express, 2011, 19, 24198.	3.4	23
335	Mid-infrared laser-driven broadband water-window supercontinuum generation from pre-excited medium. Optics Express, 2011, 19, 24376.	3.4	5
336	Broadband large-ellipticity harmonic generation with polar molecules. Optics Express, 2011, 19, 25084.	3.4	13
337	Macroscopic control of quantum paths in high order harmonics by a weak second harmonic field. Optics Express, 2011, 19, 25125.	3.4	1
338	Isolated attosecond pulse generation with the stability against the carrier-envelope phase shift and with the high-beam quality from CO gas medium. Optics Express, 2011, 19, 26174.	3.4	6
339	Wavelength dependence of electron localization in the laser-driven dissociation of H2+. Optics Express, 2011, 19, 26359.	3.4	33
340	Control the revisit time of the electron wave packet. Optics Letters, 2011, 36, 2758.	3.3	35
341	Excimer laser deposited CuO and Cu2O films with third-order optical nonlinearities by femtosecond z-scan measurement. Applied Physics A: Materials Science and Processing, 2011, 104, 171-175.	2.3	24
342	Colored conical emission in BBO crystal induced by intense femtosecond pulses. Optics Communications, 2011, 284, 670-674.	2.1	5

#	Article	IF	CITATIONS
343	Enhanced ionization of perpendicularly aligned H2 in intense laser fields. Optics Communications, 2011, 284, 2505-2508.	2.1	2
344	Third order optical susceptibilities of the Cu2O thin film. Thin Solid Films, 2011, 519, 6557-6560.	1.8	14
345	Coulomb-tail effect of electron-electron interaction on nonsequential double ionization. Physical Review A, 2011, 84, .	2.5	42
346	Phase-locked ultra-broadband supercontinuum generation in a mid-infrared polarization gating. Journal of Modern Optics, 2011, 58, 62-68.	1.3	2
347	Experimental femtosecond laser photodisruption of rabbit sclera for minimally invasive laser sclerostomy: An in vitro study. Optics and Lasers in Engineering, 2010, 48, 806-810.	3.8	3
348	Optical nonlinearities of Au/TiO2 films excited by high-repetition-rate femtosecond laser. Thin Solid Films, 2010, 519, 1346-1350.	1.8	8
349	Internuclear-distance dependence of electron correlation in nonsequential double ionization of H_2. Optics Express, 2010, 18, 9064.	3.4	27
350	Mid-infrared modulated polarization gating for ultra-broadband supercontinuum generation. Optics Express, 2010, 18, 11308.	3.4	31
351	Size-related third-order optical nonlinearities of Au nanoparticle arrays. Optics Express, 2010, 18, 13874.	3.4	73
352	Role of Coulomb focusing on the electron transverse momentum of above-threshold ionization. Optics Express, 2010, 18, 14293.	3.4	23
353	Complex sub-laser-cycle electron dynamics in strong-field nonsequential triple ionizaion. Optics Express, 2010, 18, 16025.	3.4	47
354	Intensity-dependent reversal of nonlinearity sign in a gold nanoparticle array. Optics Letters, 2010, 35, 1560.	3.3	58
355	Multiple optical Tamm states at a metal–dielectric mirror interface. Optics Letters, 2010, 35, 4112.	3.3	115
356	Controlling nonsequential double ionization via two-color few-cycle pulses. Optics Express, 2010, 18, 632.	3.4	52
357	Laser parameter influence on quantum path selection in a bichromatic field. Journal of Physics B: Atomic, Molecular and Optical Physics, 2009, 42, 105601.	1.5	6
358	Nonlinear optical properties of laser deposited CuO thin films. Thin Solid Films, 2009, 517, 4277-4280.	1.8	59
359	Third-order optical nonlinearities in anatase and rutile TiO2 thin films. Thin Solid Films, 2009, 517, 5601-5604.	1.8	71
360	Femtosecond laser deposited zinc oxide film and its optical properties. Vacuum, 2009, 83, 892-896.	3.5	11

#	Article	IF	CITATIONS
361	Controlled growth and characteristics of single-phase Cu2O and CuO films by pulsed laser deposition. Vacuum, 2009, 83, 927-930.	3.5	228
362	Polarization-dependent blue-shifted emissions in microstructure fibers. Optics Communications, 2009, 282, 640-643.	2.1	2
363	Broadband water window supercontinuum generation with a tailored mid-IR pulse in neutral media. Optics Letters, 2009, 34, 2102.	3.3	77
364	Refractive index sensor based on a microhole in single-mode fiber created by the use of femtosecond laser micromachining. Optics Letters, 2009, 34, 3328.	3.3	81
365	Few-cycle attosecond pulses with stabilized-carrier-envelope phase in the presence of a strong terahertz field. Optics Express, 2009, 17, 5139.	3.4	48
366	Manipulating nonsequential double ionization via alignment of asymmetric molecules. Optics Express, 2009, 17, 15550.	3.4	18
367	Structural properties of ZnO thin films on Si substrate using femtosecond laser deposition. Journal of Crystal Growth, 2008, 310, 551-555.	1.5	1
368	Molecular structure and visible absorption maximum of cobalt phthalocyanine: Quantum calculations via semi-empirical methods. Dyes and Pigments, 2008, 77, 277-280.	3.7	12
369	Growth and characteristics of laser deposited anatase and rutile TiO2 films on Si substrates. Thin Solid Films, 2008, 517, 745-749.	1.8	76
370	Spectrum of copper phthalocyanine: Experiments and semi-empirical quantum chemical calculations. Physica B: Condensed Matter, 2008, 403, 1704-1707.	2.7	6
371	Femtosecond filament and supercontinuum generated in cobalt phthalocyanine chloroform solution. Materials Letters, 2008, 62, 1599-1601.	2.6	1
372	Optical limiting properties of two phthalocyanines using 1064-nm laser in solution. Materials Letters, 2008, 62, 3059-3062.	2.6	26
373	Magnetic properties of carbonyl iron fibers and their microwave absorbing characterization as the filer in polymer foams. Journal of Alloys and Compounds, 2008, 456, 452-455.	5.5	50
374	Carrier-envelope phase measurement from half-cycle high harmonics. Optics Express, 2008, 16, 5868.	3.4	27
375	Method to precisely measure the phase of few-cycle laser pulses. Optics Express, 2008, 16, 6455.	3.4	8
376	Multi-cycle laser-driven broadband supercontinuum with a modulated polarization gating. Optics Express, 2008, 16, 9795.	3.4	107
377	An efficient method of all-optical buffering with ultra-small core photonic crystal fibers. Optics Express, 2008, 16, 14142.	3.4	14
378	Nonlinear absorption in CuPc-doped PMMA thin film in the femtosecond regime: Experimental and theoretical studies. Optics Express, 2008, 16, 14571.	3.4	31

#	Article	IF	CITATIONS
379	Double ionization of HeH^+ molecules in intense laser fields. Optics Express, 2008, 16, 17070.	3.4	19
380	Asymmetric molecular gating for supercontinuous high harmonic generation in the plateau. Optics Express, 2008, 16, 17542.	3.4	20
381	Phase-dependent nonsequential double ionization by few-cycle laser pulses. Journal of Physics B: Atomic, Molecular and Optical Physics, 2008, 41, 125601.	1.5	36
382	Quantum Control for Broadband Attosecond Pulse Generation. The Review of Laser Engineering, 2008, 36, 1008-1011.	0.0	0
383	Control of quantum paths in high-order harmonic generation via a ω+3ω bichromatic laser field. Journal of Physics B: Atomic, Molecular and Optical Physics, 2007, 40, 869-875.	1.5	29
384	Control of quantum paths of high-order harmonics and attosecond pulse generation in the presence of a static electric field. Journal of Physics B: Atomic, Molecular and Optical Physics, 2007, 40, 2321-2331.	1.5	54
385	Nonlinear Thomson scattering in the few-cycle regime. Journal of Physics B: Atomic, Molecular and Optical Physics, 2007, 40, 403-411.	1.5	17
386	Femtosecond laser direct fabrication of metallic microcantilevers for a micro-corrosion-fatigue test. Journal of Micromechanics and Microengineering, 2007, 17, 1307-1313.	2.6	9
387	Quasimonochromatic x-rays generated from nonlinear Thomson backscattering. Physica Scripta, 2007, 75, 195-200.	2.5	6
388	Ablation and cutting of silicon wafer and micro-mold fabrication using femtosecond laser pulses. Journal of Laser Applications, 2007, 19, 240-244.	1.7	11
389	Attosecond ionization gating for isolated attosecond electron wave packet and broadband attosecond xuv pulses. Physical Review A, 2007, 76, .	2.5	65
390	Single attosecond pulse generation from asymmetric molecules with a multicycle laser pulse. Optics Letters, 2007, 32, 1186.	3.3	31
391	Efficient isolated attosecond pulse generation from a multi-cycle two-color laser field. Optics Express, 2007, 15, 530.	3.4	41
392	Phase jitter of chirped subpicosecond solitons in a noisy optical fiber channel: Exact moment method description. Europhysics Letters, 2007, 80, 34003.	2.0	2
393	Optical characterization of β-FeSi2 thin films prepared on fused quartz by femtosecond laser ablation. Physica B: Condensed Matter, 2007, 399, 33-37.	2.7	7
394	Noncrystalline micromachining of amorphous alloys using femtosecond laser pulses. Materials Letters, 2007, 61, 4290-4293.	2.6	22
395	Morphology and oxidation of Zr-based amorphous alloy ablated by femtosecond laser pulses. Applied Physics A: Materials Science and Processing, 2007, 89, 547-552.	2.3	9
396	Synthesis of SrAl2O4 and SrAl12O19 via ethylenediaminetetraacetic acid precursor. Materials Chemistry and Physics, 2006, 98, 51-54.	4.0	13

#	Article	IF	CITATIONS
397	Synthesis of La(Mg1/2Ti1/2)O3 powder through ethylenediaminetetraacetic acid gel combustion. Ceramics International, 2006, 32, 57-60.	4.8	6
398	Attosecond X-ray pulse obtained from linear Thomson scattering. Optik, 2006, 117, 220-224.	2.9	11
399	Spectral distributions of harmonic generation from electron oscillation driven by intense femtosecond laser pulses. Optics Communications, 2006, 261, 104-108.	2.1	6
400	Morphology of femtosecond laser-induced structural changes in KTP crystal. Applied Surface Science, 2006, 253, 1443-1446.	6.1	3
401	Single-phase Î ² -FeSi2 thin films prepared on Si wafer by femtosecond laser ablation and its photoluminescence at room temperature. Physics Letters, Section A: General, Atomic and Solid State Physics, 2006, 350, 293-296.	2.1	10
402	Synthesis of yttrium aluminum garnet (YAC) from an ethylenediaminetetraacetic acid precursor. Materials Science and Engineering B: Solid-State Materials for Advanced Technology, 2006, 127, 203-206.	3.5	13
403	Synthesis of SrAl4O7 via citric acid precursor. Materials Chemistry and Physics, 2006, 95, 62-66.	4.0	24
404	Effects of pH and citric acid contents on the synthesis of BaTi4O9 via polymeric precursor. Materials Chemistry and Physics, 2006, 96, 427-432.	4.0	13
405	Spectroscopic and fluorescence decay behaviors of Yb3+-doped SiO2–PbO–Na2O–K2O glass. Journal of Luminescence, 2005, 113, 221-228.	3.1	11
406	Effects of Yb ion concentration on the spectral properties of lead silica glasses. Optics Communications, 2005, 253, 151-155.	2.1	17
407	Synthesis of SrAl12O19 via citric acid precursor. Materials Science and Engineering B: Solid-State Materials for Advanced Technology, 2005, 123, 139-142.	3.5	11
408	Synthesis of La(Mg1/2Ti1/2)O3 via citric acid precursor. Materials Chemistry and Physics, 2005, 92, 220-224.	4.0	15
409	Preparation of La(Zn0.5Ti0.5)O3 powders via citric acid precursor. Materials Letters, 2005, 59, 1914-1918.	2.6	14
410	Spatial Coherence Measurement of 13.9 nm Ni-like Ag Soft X-Ray Laser Pumped by a 1.5 ps, 20 J Laser. Japanese Journal of Applied Physics, 2003, 42, 443-448.	1.5	8
411	Demonstration of a Transient High Gain Soft X-Ray Laser for Neon-Like Argon. Japanese Journal of Applied Physics, 2002, 41, L133-L135.	1.5	8
412	Demonstration of a transient-gain nickel-like xenon-ion x-ray laser. Optics Letters, 2002, 27, 1911.	3.3	10
413	Demonstration of XUV amplification to the ground state in low-charged nitrogen ions. Optics Communications, 1999, 170, 71-78.	2.1	4
414	Time-resolved soft x-ray absorption spectroscopy of silicon using femtosecond laser plasma x rays. Applied Physics Letters, 1999, 75, 2350-2352.	3.3	52

#	Article	IF	CITATIONS
415	Spatial coherence of prepulse-induced neonlike x-ray lasers. Physical Review A, 1998, 58, 628-635.	2.5	19
416	Study of Ne- and Ni-like x-ray lasers using the prepulse technique. Physics of Plasmas, 1997, 4, 479-489.	1.9	25
417	Lasing in neonlike sulphur and silicon. Optics Communications, 1997, 133, 196-200.	2.1	21
418	Self-photopumped neonlike x-ray laser. Optics Letters, 1996, 21, 408.	3.3	19
419	Two-dimensional near-field images of the neonlike germanium soft-x-ray laser. Optics Letters, 1996, 21, 866.	3.3	14
420	Relative merits of using curved targets and the prepulse technique to enhance the output of the neon-like germanium X-ray laser. Optics Communications, 1996, 124, 287-291.	2.1	13
421	Angular energy distribution and temporal evolution of pulses emitted from low-ZneonlikeJ=0–1 x-ray lasers. Physical Review A, 1996, 54, 5193-5200.	2.5	6
422	Demonstration of x-ray lasing in nickel-like tin. Physical Review A, 1996, 53, R652-R654.	2.5	23
423	An alternative method for gain determination of recombination X-ray lasers. Optics Communications, 1994, 113, 85-90.	2.1	3
424	Time and space resolved studies of recombination x-ray lasers. Optics Communications, 1993, 102, 271-276.	2.1	1
425	Space―and timeâ€resolved investigation of short wavelength xâ€ray laser in Liâ€like Ca ions. Applied Physics Letters, 1993, 63, 1023-1025.	3.3	13
426	Thermoelectric power of single phase YBa2Cu3O7â^'x superconductors. Solid State Communications, 1988, 65, 355-358.	1.9	34
427	Thermoelectric power in three La-Ba-Cu oxides. Solid State Communications, 1987, 64, 537-539.	1.9	7